Acta Cryst E CRYSTALLOGRAPHIC COMMUNICATIONS

ISSN 2056-9890

Crystal structure and Hirshfeld surface analysis of *catena*-poly[4-amino-4*H*-1,2,4-triazol-1-ium [lead(II)-tri-μ-bromido]]

Olesia I. Kucheriv,[a]* Sergii O. Malinkin,[a] Olena Prysiazhna,[b,c] Alexandru Constantin Stoica[d] and Irina A. Golenya[a]

[a]Department of Chemistry, Taras Shevchenko National University of Kyiv, Volodymyrska St. 64, 01601 Kyiv, Ukraine, [b]Bakul Institute for Superhard Materials, National Academy of Sciences of, Ukraine, Avtozavodskaya St. 2, Kyiv 04074, Ukraine, [c]Department of Chemistry, Kyiv National University of Construction and Architecture, Povitroflotsky Ave. 31, Kyiv 03680, Ukraine, and [d]"Petru Poni" Institute of Macromolecular Chemistry, Aleea Gr. Ghica Voda 41A, 700487 Iasi, Romania. *Correspondence e-mail: olesia.kucheriv@univ.kiev.ua

Received 2 October 2025
Accepted 29 October 2025

Edited by B. Therrien, University of Neuchâtel, Switzerland

Keywords: crystal structure; organic–inorganic hybrids; one-dimensional polymeric chain; lead; triazolium cation.

CCDC reference: 2498871

Supporting information: this article has supporting information at journals.iucr.org/e

Hybrid organic—inorganic perovskites are a group of versatile materials with outstanding performance in photovoltaics, LEDs, lasers, and sensors. The hybrid organic–inorganic compound (4-amino-1,2,4-triazolium)$PbBr_3$, or $\{(C_2H_5N_4)[PbBr_3]\}_n$, crystallizes in the polar orthorhombic space group $Pna2_1$. Its structure is built from $[PbBr_6]$ octahedra with pronounced trigonal distortion, which are connected through face-sharing to form infinite one-dimensional chains extending along the *c*-axis direction. These inorganic chains are separated by 4-amino-1,2,4-triazolium cations that establish an extensive network of weak interactions, including N—H···Br hydrogen bonds as well as C—H···Br contacts and N···Pb tetrel bonds. Additionally, N—H···N interactions link neighboring organic cations. The network of intermolecular contacts was further examined using Hirshfeld surface analysis and two-dimensional fingerprint plots.

1. Chemical context

Organic–inorganic hybrid perovskites have emerged as a highly versatile class of functional materials, displaying exceptional performance in photovoltaics, light-emitting devices, lasers, and sensors (Zhao & Zhu, 2016). Their appeal arises from the combination of tunable optoelectronic properties, solution-processable fabrication, and structural flexibility that enables a wide spectrum of chemical designs (Younis *et al.*, 2021). Early research was dominated by three-dimensional perovskites such as $CH_3NH_3PbI_3$, which exhibit strong light absorption and long carrier diffusion lengths, making them highly efficient in solar energy conversion and photodetection (Quarti *et al.*, 2016). Nevertheless, the centrosymmetric crystal structures typical of 3D perovskites restrict the emergence of spontaneous polarization, limiting their utility in self-powered photodetectors and bulk photovoltaic effect-based devices (Li *et al.*, 2025).

To overcome these limitations, considerable attention has been directed toward designing polar hybrid perovskites. The introduction of symmetry-breaking distortions or large organic cations has been shown to stabilize polar structures, thereby enabling spontaneous polarization and associated functionalities (Ji *et al.*, 2019). Hybrid perovskites, with their adjustable inorganic frameworks and diverse organic cation chemistry, offer an attractive alternative route to engineer polar semiconductors with more favorable bandgaps and carrier dynamics (Xu *et al.*, 2019).

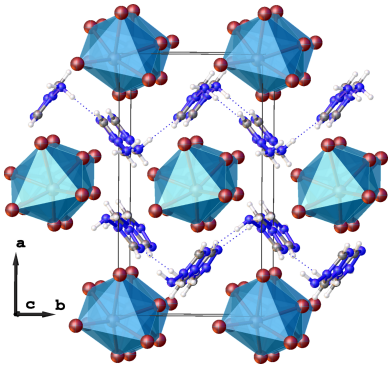

So-called low-dimensional perovskites have been particularly useful in tailoring polar structures. Two-dimensional perovskites incorporating bulky or chiral organic cations can adopt non-centrosymmetric lattices that support ferroelectricity and intrinsic bulk photovoltaic effect (Li *et al.*, 2021). Moreover, their structural distortions can induce broadband white-light emission *via* self-trapped excitons, a feature that has been linked to strong electron–phonon coupling in corrugated inorganic frameworks (Wang *et al.*, 2018). Such multifunctionality highlights the interplay between lattice distortion, optical properties, and polarity in hybrid perovskites, and it demonstrates their promise as candidates for next-generation optoelectronic devices.

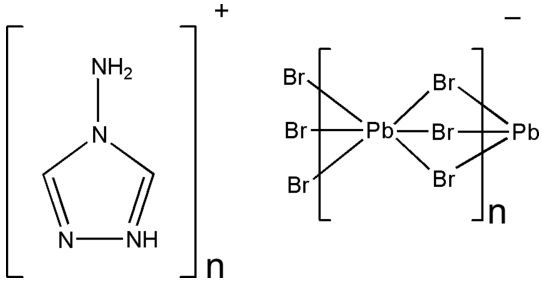

Taken together, these developments underscore the importance of polarity in hybrid perovskites for enabling novel optoelectronic phenomena and device concepts. Rational design strategies, whether through dimensional reduction, chiral templating, or cation substitution, continue to expand the library of polar perovskites with tailored bandgaps and multifunctional properties. In this context, crystallographic investigations of new polar hybrid perovskites are crucial, as they provide the structural insights necessary to understand structure–property relationships and to guide further material design. The present work contributes to this effort by reporting and analyzing the crystal structure of a new polar hybrid organic–inorganic compound (4-amino-1,2,4-triazolium)$PbBr_3$.

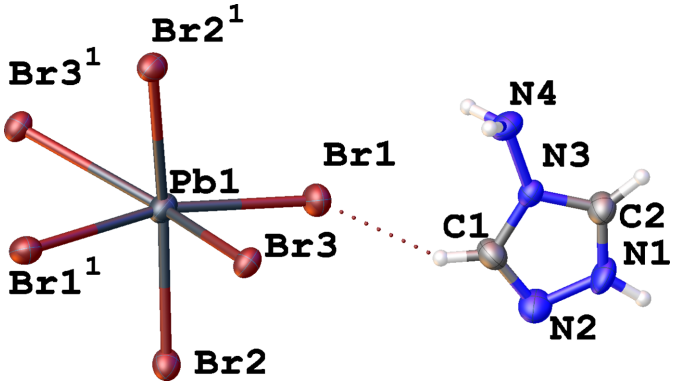

Figure 1
Fragments of (4-amino-1,2,4-triazolium)$PbBr_3$ showing the atom-labeling scheme, and a strong interaction between 4-amino-1,2,4-triazolium and the $PbBr_6$ octahedron (dotted line). Displacement ellipsoids are drawn at the 50% probability level. [Symmetry code: (1) $1-x, 1-y, -\frac{1}{2}+z$]

2. Structural commentary

The title compound crystallizes in the non-centrosymmetric space group $Pna2_1$. In this crystal structure, Pb^{2+} exhibits an octahedral coordination environment provided by six bromide anions, which features significant trigonal distortion (Fig. 1). The inorganic [$PbBr_6$] octahedra connect with each other in face-sharing manner creating infinite 1D chains which propagate along the *c*-axis direction (Fig. 2). The creation of similar faced-shared 1D chains has been previously observed for organic–inorganic hybrids with substituted imidazolium cations (Thirumurugan & Rao, 2008; Kobayashi *et al.*, 1972). The Pb—Br bond lengths are in the in the range 2.9200 (8) to 3.2563 (9) Å, the observed octahedral distortion can be quantitatively estimated by quadratic elongation parameter: $\langle\lambda_{oct}\rangle = \Sigma(l_i/l_0)^2/6 = 0.013$, where l_i are six Pb—Br bond lengths and l_0 is the average Pb—Br bond length (Robinson *et al.*, 1971). The $\sigma_\theta^2 = \Sigma(\theta_i - 90)^2/11 = 237.72$, where θ_i are twelve *cis*-Br—Pb—Br angles (Robinson *et al.*, 1971). Such a large deviation of *cis*-Br—Pb—Br angles and consequent large bond-angle variance is not very common for lead halides, though not unique, and has previously been observed for compounds that form similar face-shared 1D inorganic chains (He *et al.*, 2019; Tang & Guloy, 1999).

The inorganic 1D chains are separated by 4-amino-1,2,4-triazolium organic cations, which compensate the negative charge of the inorganic component. All bond lengths and angles in this organic cation are within the expected range (Allen *et al.*, 1987).

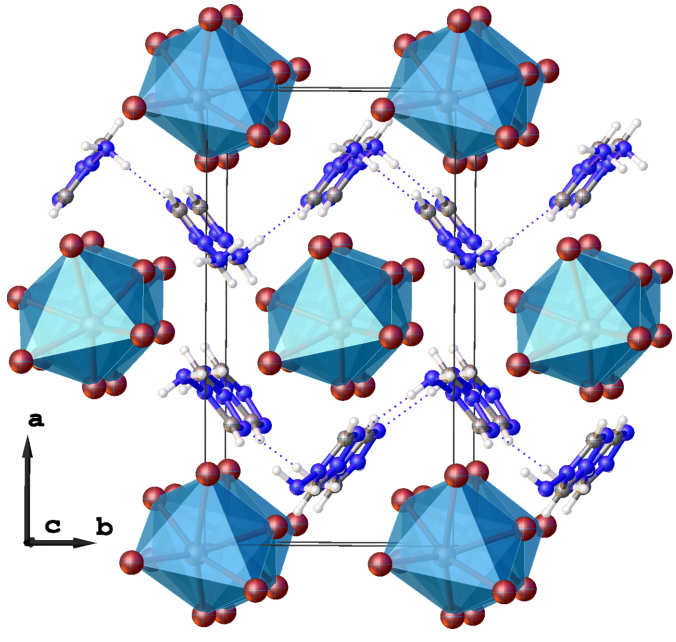

Figure 2
Fragment of the crystal structure of (4-amino-1,2,4-triazolium)$PbBr_3$ showing the propagation of the infinite one-dimensional face-shared chains along the *c*-axis direction. N—H···N hydrogen bonds are shown as blue dotted lines.

Table 1
Hydrogen-bond geometry (Å, °).

D—H···A	D—H	H···A	D···A	D—H···A
N4—H4A···Br2^{i}	0.90	2.82	3.700 (7)	167
N4—H4B···Br1	0.91	3.39	3.763 (6)	107
N4—H4B···N2^{ii}	0.91	2.30	3.203 (9)	177
N1—H1···Br2^{iii}	0.86	2.76	3.414 (7)	134
C1—H1A···Br3^{iv}	0.93	2.96	3.569 (7)	124
C1—H1A···Br1	0.93	2.96	3.711 (8)	139
C2—H2···Br3^{v}	0.93	2.85	3.424 (8)	121
C2—H2···Br2^{vi}	0.93	2.93	3.774 (8)	152

Symmetry codes: (i) $x-\frac{1}{2}, -y+\frac{3}{2}, z$; (ii) $-x+\frac{1}{2}, y-\frac{1}{2}, z-\frac{1}{2}$; (iii) $x-\frac{1}{2}, -y+\frac{3}{2}, z+1$; (iv) $-x+1, -y+1, z+\frac{1}{2}$; (v) $x-\frac{1}{2}, -y+\frac{1}{2}, z+1$; (vi) $-x+\frac{1}{2}, y-\frac{1}{2}, z+\frac{1}{2}$.

3. Supramolecular features

The organic cations interact with the inorganic 1D chains by a network of weak interactions (Fig. 3). The amino group participates in two hydrogen bonds: an N4—H4B···N2^{ii} [symmetry code: (ii) $-x+\frac{1}{2}, y-\frac{1}{2}, z-\frac{1}{2}$] contact with a neighboring aminotriazolium cation, and an N4—H4B···Br1 contact with a bromine from a neighboring inorganic polymeric chain. Detailed geometry of these hydrogen bonds can be found in Table 1. In addition, four relatively short C—H···Br contacts (all H···Br < 3.0 Å) that help consolidate the packing are observed. In addition, the Pb1···N4 distance is 3.357 (7) Å, which is significantly shorter than the sum of the van der Waals radii of the corresponding elements (4.2 Å). This short contact can be interpreted as a non-covalent tetrel bond, in which the lead atom acts as a tetrel-bond donor possessing an electrophilic region on its surface, while the nitrogen atom serves as a nucleophilic tetrel-bond acceptor with an electron pair (Varadwaj *et al.*, 2023; Scheiner, 2021).

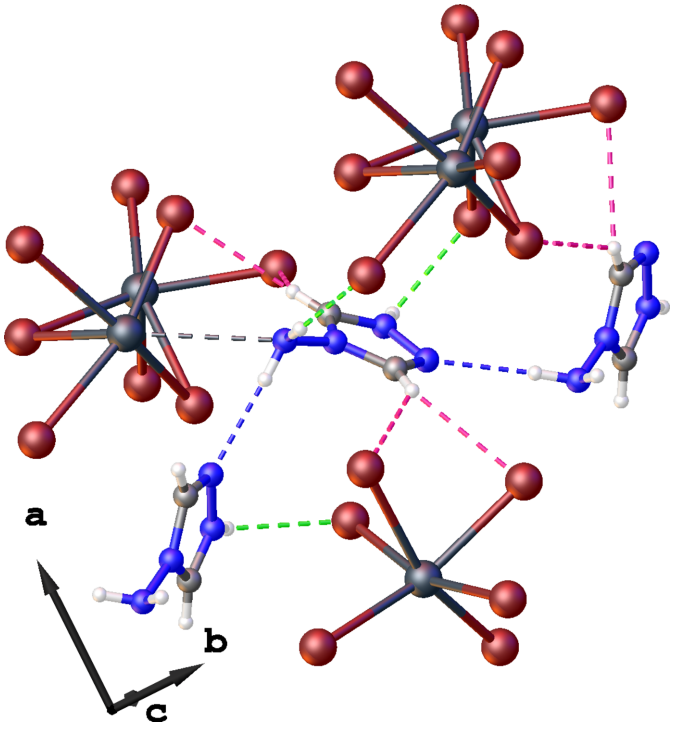

Figure 3
Weak interactions present in the structure: tetrel N···Pb bond (black dashed lines), N—H···Br (green dashed lines), N—H···N (blue dashed lines) and C—H···Br (pink dashed lines).

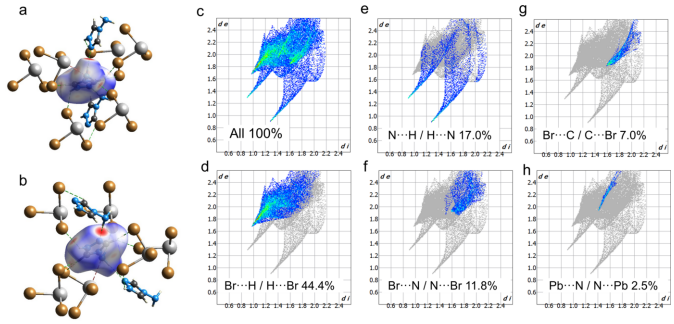

Figure 4
(*a*),(*b*) Hirshfeld surface highlighting the strength and distribution of intermolecular interactions between the organic and inorganic components of the title compound. (*c*)–(*h*) The corresponding fingerprint plots illustrating the frequency of specific intermolecular contacts within the crystal structure.

4. Hirshfeld surface analysis

Intermolecular interactions in the title compound were additionally analyzed using Hirshfeld surface and fingerprint plots obtained with *CrystalExplorer* (Spackman *et al.*, 2021). To visualize intermolecular interactions, the Hirshfeld surface was plotted with d_{norm} at the conventional resolution and rendered with a fixed color scheme (Fig. 4*a*–*b*): regions where interatomic separations approximate the sum of van der Waals radii are depicted in white, shorter contacts are highlighted in red, and longer ones in blue. The fingerprint plots depict how often these interactions appear in the crystal structure. Hence, the Hirshfeld surface and the 2D plots convey different aspects: one reflects contact strength, the other their frequency. The red regions of the Hirshfeld surface here mostly correspond to stronger N—H···Br and N—H···N contacts, while pale pink regions can be observed for —H···Br and Pb···N interactions.

The two-dimensional fingerprint plots (Fig. 4*c*–*h*) show that the most frequently observed meaningful weak interactions in the structure are Br···H/H···Br contacts, which make a 44.4% contribution to the overall number of interactions. Other contacts that make notable contributions include Br···N/N···Br (11.8%) and N···H/H···N (17.0%). Br···C/C···Br and Pb···N/N···Pb make 7.0 and 2.5% contributions, respectively. The observed Br···C/C···Br contact can be attributed to a shifted weak π···Br interaction oriented toward the C atom of the triazole ring [Br2···C1 = 3.487 (8) Å, ring centroid···C—Br = 96.8 (4)°]. The remaining interactions are H···H contacts, which occur frequently in the structure as a result of the terminal hydrogen-atom positions; nevertheless, they lack chemical significance.

5. Database survey

A survey of the Cambridge Structural Database (CSD version 5.45, update of September 2024; Groom *et al.*, 2016) revealed

that the formation of organic–inorganic compounds with $[PbBr_6]^{4-}$ octahedra that combine in a face-sharing manner is quite common (101 hits). It is specifically worth paying attention to (3-amino-1,2,4-triazolato)$PbBr_3$, which is isostructural with the title compound (Li *et al.*, 2007). The 4-amino-1,2,4-triazolium cation has already been used for the formation of the organic–inorganic hybrid compound bis(4-amino-1,2,4-triazolium) hexachloridostannate(IV) (Daszkiewicz & Marchewka, 2012).

6. Synthesis and crystallization

$PbBr_2$ (18.3 mg, 0.05 mmol) was dissolved in 0.2 ml of conc. HBr (48%). Then, 4-amino-1,2,4-triazole (21.0 mg, 0.25 mmol) was added to the former solution. Colorless crystals formed on the bottom of the vial within 24 h and were stored in the mother solution prior to SXRD analysis.

7. Refinement

Crystal data, data collection and structure refinement details are summarized in Table 2. H atoms were placed at calculated positions and refined isotropically with $U_{iso}(H) = 1.2U_{eq}(C)$ or $1.2U_{eq}(N)$. H atoms of the aromatic ring were placed on the external bisector of the $X—C—Y$ or $X—N—Y$ angle and refined as riding. The H atoms of the amino group were positioned with an idealized geometry (NH_2, hydrogens lying in the plane of the nearest substituent) and refined as riding.

Table 2
Experimental details.

Crystal data	
Chemical formula	$(C_2H_5N_4)[PbBr_3]$
M_r	532.02
Crystal system, space group	Orthorhombic, $Pna2_1$
Temperature (K)	293
a, b, c (Å)	14.4941 (3), 7.9506 (2), 8.0569 (2)
V (Å^3)	928.45 (4)
Z	4
Radiation type	Mo $K\alpha$
μ (mm^{-1})	31.02
Crystal size (mm)	0.26 × 0.13 × 0.09
Data collection	
Diffractometer	XtaLAB Synergy, Dualflex, HyPix
Absorption correction	Analytical (*CrysAlis PRO*; Rigaku OD, 2024)
T_{min}, T_{max}	0.022, 0.149
No. of measured, independent and observed [$I > 2\sigma(I)$] reflections	11100, 2209, 2054
R_{int}	0.043
$(\sin\theta/\lambda)_{max}$ (Å^{-1})	0.709
Refinement	
$R[F^2 > 2\sigma(F^2)]$, $wR(F^2)$, S	0.022, 0.047, 1.03
No. of reflections	2209
No. of parameters	92
No. of restraints	1
H-atom treatment	H-atom parameters constrained
$\Delta\rho_{max}$, $\Delta\rho_{min}$ (e Å^{-3})	1.08, −1.00
Absolute structure	Flack x determined using 769 quotients $[(I^+)-(I^-)]/[(I^+)+(I^-)]$ (Parsons *et al.*, 2013)
Absolute structure parameter	−0.025 (7)

Computer programs: *CrysAlis PRO* (Rigaku OD, 2024), *SHELXT2018/2* (Sheldrick, 2015*a*), *SHELXL2019/3* (Sheldrick, 2015*b*) and *OLEX2* (Dolomanov *et al.*, 2009).

Acknowledgements

The authors are grateful to the FAIRE programme provided by the Cambridge Crystallographic Data Centre (CCDC) for the opportunity to use the Cambridge Structural Database (CSD) and associated software.

Funding information

Funding for this research was provided by: Ministry of education and science of Ukraine (grant No. 24BF037-01M).

References

Allen, F. H., Kennard, O., Watson, D. G., Brammer, L., Orpen, A. G. & Taylor, R. (1987). *J. Chem. Soc. Perkin Trans. 2* pp. S1–S19.

Daszkiewicz, M. & Marchewka, M. K. (2012). *J. Mol. Struct.* **1017**, 90–97.

Dolomanov, O. V., Bourhis, L. J., Gildea, R. J., Howard, J. A. K. & Puschmann, H. (2009). *J. Appl. Cryst.* **42**, 339–341.

Groom, C. R., Bruno, I. J., Lightfoot, M. P. & Ward, S. C. (2016). *Acta Cryst.* B**72**, 171–179.

He, Y., Huang, Y.-R., Li, Y.-L., Li, H.-H., Chen, Z.-R. & Jiang, R. (2019). *Inorg. Chem.* **58**, 13862–13880.

Ji, C., Wang, S., Li, L., Sun, Z., Hong, M. & Luo, J. (2019). *Adv. Funct. Mater.* **29**, 1805038.

Kobayashi, M., Marumo, F. & Saito, Y. (1972). *Acta Cryst.* B**28**, 470–474.

Li, D., Wu, W., Han, S., Liu, X., Peng, Y., Li, X., Li, L., Hong, M. & Luo, J. (2021). *Chem. Sci.* **12**, 3050–3054.

Li, H., Wang, Z., Guan, Q., Ji, C., Li, R., Ye, H., Wu, Z., Zhang, C. & Luo, J. (2025). *Angew. Chem. Int. Ed.* **64**, e202500765.

Li, Y., Lin, C., Zheng, G. & Lin, J. (2007). *J. Solid State Chem.* **180**, 173–179.

Parsons, S., Flack, H. D. & Wagner, T. (2013). *Acta Cryst.* B**69**, 249–259.

Quarti, C., Mosconi, E., Ball, J. M., D'Innocenzo, V., Tao, C., Pathak, S., Snaith, H. J., Petrozza, A. & De Angelis, F. (2016). *Energy Environ. Sci.* **9**, 155–163.

Rigaku OD (2024). *CrysAlis PRO*. Rigaku Oxford Diffraction, Yarnton, England.

Robinson, K., Gibbs, G. V. & Ribbe, P. H. (1971). *Science* **172**, 567–570.

Scheiner, S. (2021). *Phys. Chem. Chem. Phys.* **23**, 5702–5717.

Sheldrick, G. M. (2015*a*). *Acta Cryst.* A**71**, 3–8.

Sheldrick, G. M. (2015*b*). *Acta Cryst.* C**71**, 3–8.

Spackman, P. R., Turner, M. J., McKinnon, J. J., Wolff, S. K., Grimwood, D. J., Jayatilaka, D. & Spackman, M. A. (2021). *J. Appl. Cryst.* **54**, 1006–1011.

Tang, Z. & Guloy, A. M. (1999). *J. Am. Chem. Soc.* **121**, 452–453.

Thirumurugan, A. & Rao, C. N. R. (2008). *Cryst. Growth Des.* **8**, 1640–1644.

Varadwaj, P. R., Varadwaj, A., Marques, H. M. & Yamashita, K. (2023). *CrystEngComm* **25**, 1411–1423.

Wang, S., Yao, Y., Kong, J., Zhao, S., Sun, Z., Wu, Z., Li, L. & Luo, J. (2018). *Chem. Commun.* **54**, 4053–4056.

Xu, W.-J. J., Kopyl, S., Kholkin, A. & Rocha, J. (2019). *Coord. Chem. Rev.* **387**, 398–414.

Younis, A., Lin, C., Guan, X., Shahrokhi, S., Huang, C., Wang, Y., He, T., Singh, S., Hu, L., Retamal, J. R. D., He, J. & Wu, T. (2021). *Adv. Mater.* **33**, 2005000.

Zhao, Y. & Zhu, K. (2016). *Chem. Soc. Rev.* **45**, 655–689.

supporting information

Acta Cryst. (2025). E**81**, 1115-1118 [https://doi.org/10.1107/S2056989025009557]

Crystal structure and Hirshfeld surface analysis of *catena*-poly[4-amino-4*H*-1,2,4-triazol-1-ium [lead(II)-tri-μ-bromido]]

Olesia I. Kucheriv, Sergii O. Malinkin, Olena Prysiazhna, Alexandru Constantin Stoica and Irina A. Golenya

Computing details

***catena*-Poly[4-amino-4*H*-1,2,4-triazol-1-ium [lead(II)-tri-μ-bromido]]**

Crystal data

$(C_2H_5N_4)[PbBr_3]$
$M_r = 532.02$
Orthorhombic, $Pna2_1$
$a = 14.4941$ (3) Å
$b = 7.9506$ (2) Å
$c = 8.0569$ (2) Å
$V = 928.45$ (4) Å^3
$Z = 4$
$F(000) = 928$
$D_x = 3.806$ Mg m^{-3}
Mo $K\alpha$ radiation, $\lambda = 0.71073$ Å
Cell parameters from 7167 reflections
$\theta = 2.8$–$29.6°$
$\mu = 31.02$ mm^{-1}
$T = 293$ K
Prism, clear light colourless
0.26 × 0.13 × 0.09 mm

Data collection

XtaLAB Synergy, Dualflex, HyPix diffractometer
Radiation source: micro-focus sealed X-ray tube, PhotonJet (Mo) X-ray Source
Mirror monochromator
Detector resolution: 10.0000 pixels mm^{-1}
ω scans
Absorption correction: analytical (CrysAlisPro; Rigaku OD, 2024)
$T_{min} = 0.022$, $T_{max} = 0.149$
11100 measured reflections
2209 independent reflections
2054 reflections with $I > 2\sigma(I)$
$R_{int} = 0.043$
$\theta_{max} = 30.3°$, $\theta_{min} = 2.8°$
$h = -18\rightarrow20$
$k = -9\rightarrow10$
$l = -10\rightarrow10$

Refinement

Refinement on F^2
Least-squares matrix: full
$R[F^2 > 2\sigma(F^2)] = 0.022$
$wR(F^2) = 0.047$
$S = 1.03$
2209 reflections
92 parameters
1 restraint
Primary atom site location: dual
Hydrogen site location: mixed
H-atom parameters constrained
$w = 1/[\sigma^2(F_o^2) + (0.0251P)^2]$ where $P = (F_o^2 + 2F_c^2)/3$
$(\Delta/\sigma)_{max} = 0.001$
$\Delta\rho_{max} = 1.08$ e Å^{-3}
$\Delta\rho_{min} = -1.00$ e Å^{-3}
Extinction correction: SHELXL-2019/2 (Sheldrick 2015b), $Fc^*=kFc[1+0.001xFc^2\lambda^3/\sin(2\theta)]^{-1/4}$
Extinction coefficient: 0.0094 (3)
Absolute structure: Flack *x* determined using 769 quotients $[(I^+)-(I^-)]/[(I^+)+(I^-)]$ (Parsons *et al.*, 2013)
Absolute structure parameter: −0.025 (7)

Special details

Geometry. All esds (except the esd in the dihedral angle between two l.s. planes) are estimated using the full covariance matrix. The cell esds are taken into account individually in the estimation of esds in distances, angles and torsion angles; correlations between esds in cell parameters are only used when they are defined by crystal symmetry. An approximate (isotropic) treatment of cell esds is used for estimating esds involving l.s. planes.

Fractional atomic coordinates and isotropic or equivalent isotropic displacement parameters (Å²)

	x	*y*	*z*	U_{iso}*/U_{eq}
Pb1	0.47953 (2)	0.53836 (3)	0.04097 (4)	0.03289 (11)
Br3	0.53855 (5)	0.23101 (10)	0.20857 (10)	0.02956 (17)
Br2	0.59827 (5)	0.72427 (10)	0.28638 (10)	0.03375 (18)
Br1	0.34324 (5)	0.52673 (11)	0.32075 (11)	0.0375 (2)
N3	0.1648 (4)	0.4808 (8)	0.7102 (8)	0.0249 (12)
N4	0.1308 (4)	0.4089 (9)	0.5628 (9)	0.0344 (14)
H4A	0.125107	0.485825	0.481111	0.041*
H4B	0.167219	0.328072	0.517335	0.041*
N1	0.1775 (5)	0.5361 (9)	0.9650 (9)	0.0386 (16)
H1	0.167398	0.537000	1.070146	0.046*
N2	0.2468 (4)	0.6217 (10)	0.8918 (8)	0.0408 (17)
C1	0.2371 (5)	0.5858 (11)	0.7359 (10)	0.0375 (18)
H1A	0.275035	0.627032	0.652065	0.045*
C2	0.1270 (6)	0.4510 (10)	0.8579 (10)	0.0356 (18)
H2	0.075805	0.384404	0.880651	0.043*

Atomic displacement parameters (Å²)

	U^{11}	U^{22}	U^{33}	U^{12}	U^{13}	U^{23}
Pb1	0.04173 (17)	0.03125 (16)	0.02568 (15)	−0.00392 (10)	−0.00250 (14)	0.00146 (16)
Br3	0.0395 (3)	0.0267 (4)	0.0225 (3)	0.0010 (3)	−0.0002 (3)	0.0003 (3)
Br2	0.0404 (4)	0.0298 (4)	0.0311 (4)	−0.0070 (3)	0.0042 (3)	−0.0012 (3)
Br1	0.0335 (4)	0.0457 (5)	0.0333 (4)	−0.0013 (3)	0.0056 (3)	−0.0005 (4)
N3	0.028 (3)	0.027 (3)	0.020 (3)	0.003 (2)	0.001 (2)	0.000 (2)
N4	0.044 (3)	0.034 (3)	0.026 (4)	−0.001 (3)	−0.005 (3)	−0.005 (3)
N1	0.057 (4)	0.040 (5)	0.019 (3)	−0.005 (3)	0.008 (3)	−0.002 (3)
N2	0.051 (4)	0.035 (5)	0.037 (4)	−0.008 (3)	0.001 (3)	−0.007 (3)
C1	0.033 (4)	0.040 (5)	0.039 (5)	−0.009 (3)	0.004 (3)	−0.004 (4)
C2	0.041 (4)	0.036 (5)	0.030 (4)	−0.005 (3)	0.006 (3)	−0.005 (3)

Geometric parameters (Å, º)

Pb1—Br3	2.9200 (8)	N4—H4A	0.9022
Pb1—Br2	3.0094 (8)	N4—H4B	0.9082
Pb1—Br2^{i}	3.1367 (8)	N1—H1	0.8600
Pb1—Br1^{i}	3.1646 (9)	N1—N2	1.348 (10)
Pb1—Br1	2.9987 (8)	N1—C2	1.319 (11)
N3—N4	1.407 (9)	N2—C1	1.296 (10)
N3—C1	1.356 (10)	C1—H1A	0.9300

N3—C2	1.332 (11)	C2—H2	0.9300
Br3—Pb1—Br2^{i}	81.41 (2)	C2—N3—C1	106.9 (7)
Br3—Pb1—Br2	86.54 (2)	N3—N4—H4A	111.8
Br3—Pb1—Br1^{i}	83.37 (2)	N3—N4—H4B	115.1
Br3—Pb1—Br1	79.61 (2)	H4A—N4—H4B	103.8
Br2—Pb1—Br2^{i}	164.197 (10)	N2—N1—H1	123.6
Br2^{i}—Pb1—Br1^{i}	79.41 (2)	C2—N1—H1	123.6
Br2—Pb1—Br1^{i}	89.11 (2)	C2—N1—N2	112.7 (7)
Br1—Pb1—Br2^{i}	103.55 (2)	C1—N2—N1	103.5 (6)
Br1—Pb1—Br2	84.14 (2)	N3—C1—H1A	124.2
Br1—Pb1—Br1^{i}	162.02 (2)	N2—C1—N3	111.5 (7)
Pb1—Br3—Pb1^{ii}	83.426 (19)	N2—C1—H1A	124.2
Pb1—Br2—Pb1^{ii}	84.095 (18)	N3—C2—H2	127.3
Pb1—Br1—Pb1^{ii}	83.786 (18)	N1—C2—N3	105.4 (7)
C1—N3—N4	130.5 (6)	N1—C2—H2	127.3
C2—N3—N4	122.5 (6)		
N4—N3—C1—N2	−179.0 (7)	C1—N3—C2—N1	−0.7 (9)
N4—N3—C2—N1	179.0 (7)	C2—N3—C1—N2	0.6 (10)
N1—N2—C1—N3	−0.3 (10)	C2—N1—N2—C1	−0.1 (10)
N2—N1—C2—N3	0.5 (9)		

Symmetry codes: (i) −*x*+1, −*y*+1, *z*−1/2; (ii) −*x*+1, −*y*+1, *z*+1/2.

Hydrogen-bond geometry (Å, º)

D—H···*A*	*D*—H	H···*A*	*D*···*A*	*D*—H···*A*
N4—H4*A*···Br2^{iii}	0.90	2.82	3.700 (7)	167
N4—H4*B*···Br1	0.91	3.39	3.763 (6)	107
N4—H4*B*···N2^{iv}	0.91	2.30	3.203 (9)	177
N1—H1···Br2^{v}	0.86	2.76	3.414 (7)	134
C1—H1*A*···Br3^{ii}	0.93	2.96	3.569 (7)	124
C1—H1*A*···Br1	0.93	2.96	3.711 (8)	139
C2—H2···Br3^{vi}	0.93	2.85	3.424 (8)	121
C2—H2···Br2^{vii}	0.93	2.93	3.774 (8)	152

Symmetry codes: (ii) −*x*+1, −*y*+1, *z*+1/2; (iii) *x*−1/2, −*y*+3/2, *z*; (iv) −*x*+1/2, *y*−1/2, *z*−1/2; (v) *x*−1/2, −*y*+3/2, *z*+1; (vi) *x*−1/2, −*y*+1/2, *z*+1; (vii) −*x*+1/2, *y*−1/2, *z*+1/2.